

Design and characterization of an SQUID microwave amplifier with impedance transformers

Junhao Hou(侯俊豪), Liliang Ying(应利良), Wei Peng(彭炜), Wentao Wu(伍文涛), Zhirong Lin(林志荣)

Citation: Chin. Phys. B. 35, 098501 (2026). DOI: 10.1088/1674-1056/ae1819 |
CSTR: 32038.14.CPB.ae1819
http://cpb.iphy.ac.cn; http://iopscience.iop.org/cpb

What follows is a list of articles you may be interested in

Increasing linear flux range of SQUID amplifier using self-feedback effect

Ying-Yu Chen(陈滢宇), Chao-Qun Wang(王超群), Yuan-Xing Xu(徐元星), Yue Zhao(赵越), Li-Liang Ying(应利良), Hang-Xing Xie(谢颃星), Bo Gao(高波), Zhen Wang(王镇)
Chin. Phys. B. 32, 118501 (2023). DOI: 10.1088/1674-1056/acd8ac

Development of series SQUID array with on-chip filter for TES detector

Wentao Wu(伍文涛), Zhirong Lin(林志荣), Zhi Ni(倪志), Peizhan Li(李佩展), Tiantian Liang(梁恬恬), Guofeng Zhang(张国峰), Yongliang Wang(王永良), Liliang Ying(应利良), Wei Peng(彭炜), Wen Zhang(张文), Shengcai Shi(史生才), Lixing You(尤立星), Zhen Wang(王镇)
Chin. Phys. B. 31, 028504 (2022). DOI: 10.1088/1674-1056/ac2b91

Fabrication of Josephson parameter amplifier and its applicationin squeezing vacuum fluctuations

Pengtao Song(宋鹏涛), Xueyi Guo(郭学仪), Kai Xu(许凯), Xiaohui Song(宋小会), Zhan Wang(王战), Zhongcheng Xiang(相忠诚), Hekang Li(李贺康), Luhong Su(苏鹭红), Yirong Jin(金贻荣), Dongning Zheng(郑东宁)
Chin. Phys. B. 30, 128502 (2021). DOI: 10.1088/1674-1056/ac0796

Fabrication and characterization of all-Nb lumped-element Josephson parametric amplifiers

Hang Xue(薛航), Zhirong Lin(林志荣), Wenbing Jiang(江文兵), Zhengqi Niu(牛铮琦), Kuang Liu(刘匡), Wei Peng(彭炜), Zhen Wang(王镇)
Chin. Phys. B. 30, 068503 (2021). DOI: 10.1088/1674-1056/abeee6

Modulation depth of series SQUIDs modified by Josephson junction area

Jie Liu(刘杰), He Gao(高鹤), Gang Li(李刚), Zheng Wei Li(李正伟), Kamal Ahmada, Zhang Ying Shan(刘建设), Jian She Liu(陈炜), Wei Chen(陈炜)
Chin. Phys. B. 26, 098501 (2017). DOI: 10.1088/1674-1056/26/9/098501

Design and characterization of an SQUID microwave amplifier with impedance transformers

Junhao Hou(侯俊豪)[1], Liliang Ying(应利良)[2,3], Wei Peng(彭炜)[2,3], Wentao Wu(伍文涛)[2,3,†], and Zhirong Lin(林志荣)[1,2,3,‡]

[1] *Shanghai University, Shanghai* 200444, *China*
[2] *State Key Laboratory of Materials for Integrated Circuits, Shanghai Institute of Microsystem and Information Technology, Chinese Academy of Sciences, Shanghai* 200050, *China*
[3] *Shanghai Key Laboratory of Superconductor Integrated Circuits Technology, Shanghai Institute of Microsystem and Information Technology, Chinese Academy of Sciences, Shanghai* 200050, *China*

(Received 1 August 2025; revised manuscript received 19 October 2025; accepted manuscript online 28 October 2025)

High-performance cryogenic amplifiers are essential components for quantum information technology and astronomical observation. In this work, we report the design and characterization of a microwave amplifier based on a superconducting quantum interference device (SQUID). The design incorporates input and output impedance transformers to center the operating frequency at approximately 5.5 GHz for specific applications. Preliminary characterization at a bath temperature of 4.2 K demonstrates a peak gain of 10.79 dB at 5.39 GHz and a saturation power of approximately −115 dBm.

Keywords: SQUID microwave amplifier, impedance transformer, superconducting amplifier

PACS: 85.25.Dq, 84.30.Le

DOI: 10.1088/1674-1056/ae1819 **CSTR:** 32038.14.CPB.ae1819

1. Introduction

The superconducting quantum interference device (SQUID) is unrivaled as a sensitive magnetic flux sensor. Its exceptional flux sensitivity, quantum-limited noise performance, and bandwidth extending to several gigahertz have made it indispensable for astronomical observation,[1–5] low-temperature physics, and superconducting quantum computing.[6–9] Compared to conventional cryogenic semiconductor amplifiers like high electron mobility transistors (HEMTs), SQUID amplifiers offer quantum-limited noise performance and also have power dissipation as much as four orders of magnitude lower than HEMT amplifiers.[10,11] Furthermore, in contrast to superconducting parametric amplifiers such as Josephson parametric amplifiers (JPAs) and traveling-wave parametric amplifiers (TWPAs),[12] SQUID amplifiers may provide superior operational simplicity by eliminating the need for an external pump signal.[13] Additionally, SQUID arrays configured in series or parallel may offer a promising approach to increase both the saturation power and operational bandwidth, further broadening their applications.[14,15] Table 1 summarizes the typical performance characteristics of the amplifiers.

The frequency range of 4 GHz–8 GHz has emerged as critically important for various quantum measurement applications.[16] We therefore concentrate the SQUID amplifier design on this specific band and develop an SQUID microwave amplifier based on microwave and circuit simulation tools. The design incorporates tailored impedance transformer networks to precisely center the operating frequency for target applications. The input network employs a 0.16-pF coupling capacitor and a 1.6-pF shunt capacitor to ensure signal coupling into the SQUID input coil efficiently. Meanwhile, the output integrates a multipole transformer to achieve optimal impedance matching with a 50-Ω transmission line.

Table 1. The typical performance characteristics of the amplifiers. The values presented in the table are typical.

	JPAs	SQUID Amp.	HEMTs
Noise temperature (K)	0.1	0.1	>1
Power dissipation	0	0	mW
Gain (dB)	20	20	35
Operating frequency	GHz	MHz–GHz	GHz
Saturation power (dBm)	–110	–110	–45

2. Design and fabrication

The design approach systematically employs microwave and circuit simulation tools, which can be summarized in three key steps. Firstly, to ensure high-performance operation, we need to make a balance between the damping parameter β_c, the screening parameter β_L,[17] and the intrinsic gain G. These three key parameters fundamentally determine the SQUID-unit geometry, as the key component of the SQUID microwave amplifier, including the input-coil turns, washer

†Corresponding author. E-mail: wentaowu@mail.sim.ac.cn
‡Corresponding author. E-mail: zrlin@mail.sim.ac.cn

© 2026 Chinese Physical Society and IOP Publishing Ltd. All rights, including for text and data mining, AI training, and similar technologies, are reserved.

dimensions, and Josephson junction specifications. Subsequently, for the microwave simulation phase, we implement the physical SQUID-unit layout in the microwave simulation tool and obtain the device's S-parameters. In this simulation, Josephson junctions (JJs) are modeled using the resistively and capacitively-shunted junction (RCSJ) approach, in which each Josephson junction is represented by a shunted resistor R_n in parallel with a junction capacitor C_j. Finally, the extracted S-parameters are imported into a circuit simulator to optimize the lumped-element impedance transformer networks. The optimized topology comprises an input network with a series coupling capacitor $C_{in} = 0.16$ pF and a shunt capacitor $C_1 = 1.6$ pF, while the output network is a π-network with two grounded capacitors C_2, C_3, and a series inductor L_1. To evaluate the influence of key parameters, we performed a simulation study on the input coupling capacitance C_{in}. It was observed that an increase in C_{in} results in a decrease in gain and an expansion in bandwidth. The gain referred to here is that provided by the impedance transformers. The simulation results are presented in Fig. 1. To clearly demonstrate the influence on gain, the S_{21} data are normalized to their maximum value.

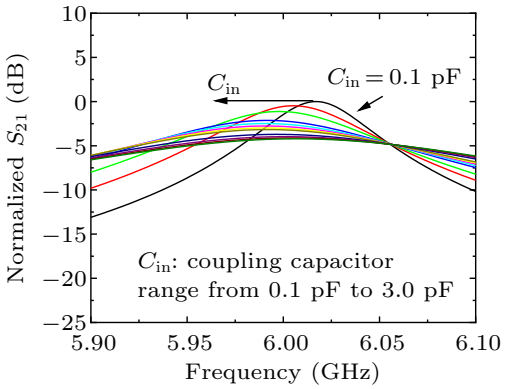


Fig. 1. Effect of the C_{in} on gain and bandwidth.

Since the RCSJ model is used for Josephson junctions in the simulation, the intrinsic gain of the device could not be simulated. However, it has been theoretically calculated using the following formula:[18]

$$G_v = \frac{M_i V_\Phi}{Z_T},$$

where $M_i = 400$ pH is the mutual inductance, $V_\Phi \sim 300\ \mu V/\Phi_0$ is the peak flux-to-voltage transfer coefficient, and Z_T is the input impedance obtained by simulation. Substituting the values yields an intrinsic gain of 17.73 dB for the device.

The optical micrograph and lumped-element equivalent circuit representation of the fabricated SQUID microwave amplifier are presented in Fig. 2. All lumped elements are physically realized as parallel-plate capacitors and planar spiral inductors. To validate the effectiveness of the impedance transformers, we conduct comparative simulations of the S_{21} parameter with and without impedance transformers. Figure 2 depicts the reference plane locations (AA'/BB' and CC'/DD') used for the S-parameter characterization. The reference planes AA'/BB' correspond to the SQUID unit without impedance transformers, while the planes CC'/DD' correspond to the SQUID unit with the optimized impedance transformers. The simulation results are illustrated in Fig. 3. To clearly demonstrate the tuning effect, the S_{21} data are normalized to their respective maximum values, indicating that the impedance transformers successfully tune the operating frequency from 7 GHz to the target 5.5 GHz.

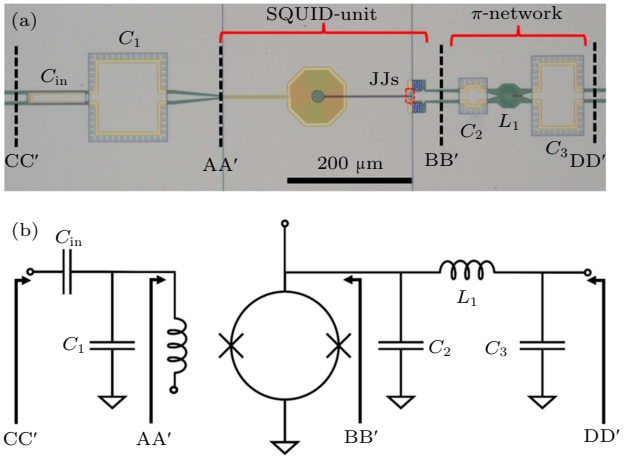


Fig. 2. (a) Optical micrograph and (b) lumped-element equivalent circuit representation of the fabricated SQUID microwave amplifier. Reference planes AA'/BB' correspond to the SQUID-unit without impedance transformers, and planes CC'/DD' correspond to the circuit with impedance transformers.

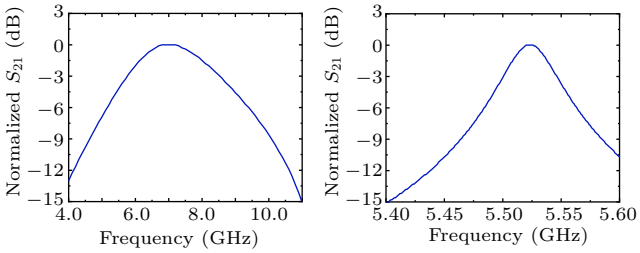


Fig. 3. Simulation of S_{21}: (a) without impedance transformers, (b) with impedance transformers. All data normalized to respective maximum values.

The SQUID-unit component primarily consists of an octagonal washer and an input coil. The washer features a 2-μm-wide slit and a hole size of 20 μm. The input coil is implemented as an open-circuit spiral structure with 16 turns of 1-μm-wide Nb lines and gaps. The SQUID loop incorporates two 3 μm×3 μm square JJs fabricated using Nb/Al–AlO_x/Nb trilayer technology. With a critical current density of $j_c = 100$ A/cm^2 at a temperature of 4.2 K,[19] each junction exhibits a critical current $I = 9$ μA. To suppress hysteretic effects, each junction is shunted with a 10-Ω resistor, yielding a damping parameter $\beta_c = 0.71$. The complete device was fabricated at the Shanghai Institute of Microsystem and Information Technology's Superconducting Electron-

ics Facility (SELF), and the whole fabrication details are available in Ref. [20]; we only summarize the patterning process of Nb/Al–AlO_x/Nb trilayer here, which involved three steps. First, the Nb counter electrode is patterned into the junction size using an i-line stepper and etched using inductively coupled plasma (ICP) etching. Subsequently, the Al–AlO_x layer is etched using IBE. The bottom Nb layer is then patterned to form the SQUID washer and establish electrical connections with the TiPd layer and the SQUID interconnections. An SiO_2 layer is then deposited over the trilayer by PECVD and etched using RIE to create contact holes. In the next step, the Nb film wiring layer is deposited and patterned to form the input coil and the JJ leads. Table 2 summarizes the key design parameters of the SQUID amplifier.

Table 2. Design parameters of SQUID microwave amplifier.

Parameter	Designed value
Area of JJ	3 μm×3 μm
Critical current density of JJ j_c	100 A/cm^2
Critical current of SQUID I_c	18 μA
Inductance of SQUID L_s	100 pH
Screening parameter β_L	0.87
Damping parameter β_c	0.71
Input coil turns N	16
Shunted resistance R_n	10 Ω
Coupling capacitor C_{in}	0.16 pF
Shunt capacitor C_1	1.6 pF
C_2 of the π-network	0.12 pF
C_3 of the π-network	0.82 pF
L_1 of the π-network	0.64 nH

3. Measurement

All measurements of the SQUID microwave amplifier were carried out at 4.2 K in a liquid helium immersion cryostat. The SQUID chip was glued on a copper-based sample box with a custom PCB as shown in Fig. 4(a). Short aluminum (Al) wire bonds connected the PCB to the chip's input and output pads, while multiple bonds shorted the washer to ground. The sample box was mounted on a liquid helium dip probe and enclosed within a superconducting Nb shield can.

At the base temperature, we systematically characterized both current-voltage-flux ($IV\Phi$) characteristics and microwave performance. The $IV\Phi$ curves of the SQUID device were particularly susceptible to noise and external interference. To address these, we employed a four-wire setup to suppress common-mode interference and measure the differential voltage across the device accurately. Additionally, low-pass filters were implemented in all DC lines to attenuate both DC source meter noise and stray RF signals. Bias current and flux bias were supplied via Yokogawa GS200 current sources routed through room-temperature filters. Figure 4(b) presents the measured V–Φ characteristics for several bias currents. From the V–Φ curves, we observed a minor distortion which arises from tight inductive coupling between the input coil and the SQUID loop. The results demonstrate a maximum voltage swing of approximately 70 μV at a bias current of 16 μA, corresponding to a peak flux-to-voltage transfer coefficient $V_\Phi \sim 300\ \mu V/\Phi_0$.

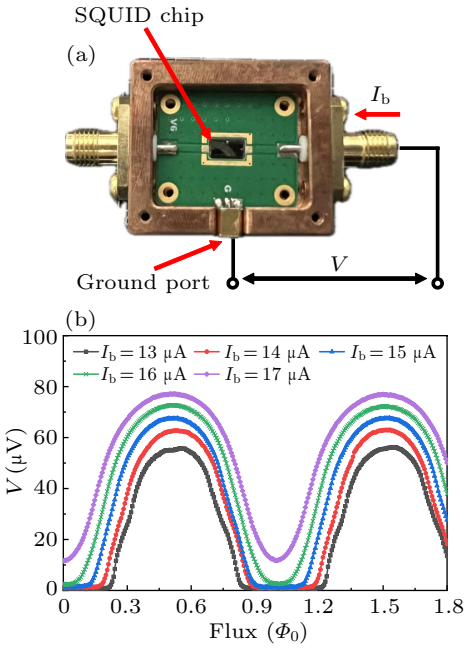


Fig. 4. (a) Photograph of the copper-based sample box, I_b is the bias current, V is the voltage across the device; (b) V–Φ characteristics of the SQUID amplifier at various bias currents.

The forward gain of the SQUID microwave amplifier was achieved from S-parameter measurements performed with a vector network analyzer (VNA). The microwave measurement setup incorporated 100 dB of input attenuation to suppress room-temperature noise and incident signals, as well as a cryogenic HEMT post-amplifier with a gain of ∼ 30 dB at 5.5 GHz. Figure 5 presents the microwave measurement chain of the SQUID amplifier.

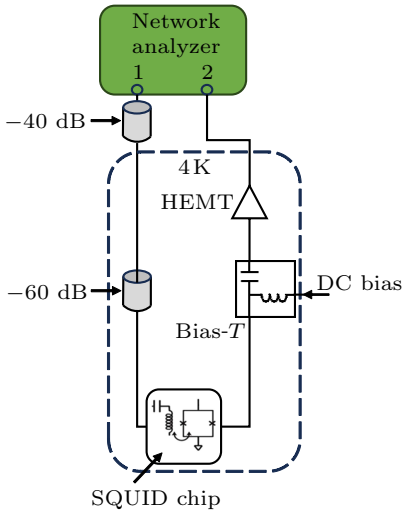


Fig. 5. Schematic representation of the microwave measurement chain.

To ensure measurement accuracy, a comprehensive calibration was performed to account for insertion losses from additional circuitry. This calibration was performed by replacing the SQUID sample box with a short coaxial reference piece, yielding a baseline S_{21}. The calibrated gain of the amplifier was then estimated by subtracting the baseline S_{21} from the S_{21} data obtained with the SQUID amplifier in the circuit.

For a microwave characterization measurement, a weak input signal of approximately −130 dBm was applied from the network analyzer. The V–Φ characteristics were initially measured to identify the optimal operating point. At the optimized bias condition of 16-μA bias current and 0.25-Φ_0 flux bias, the SQUID amplifier offers a maximum gain of 10.79 dB at 5.39 GHz with a bandwidth of 142 MHz. The measured gain results as well as the V–Φ characteristic and the optimal operating point are presented in Fig. 6. The gain variation of approximately 1 dB within the operational band likely originates from impedance mismatch at wire bond interconnects.

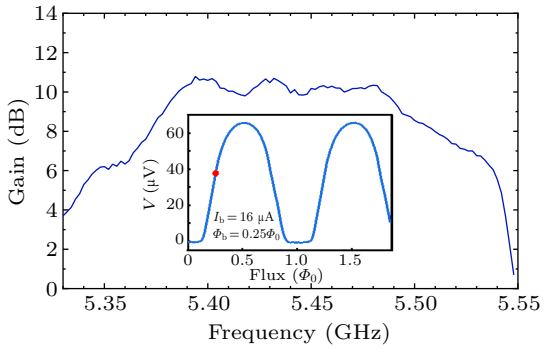


Fig. 6. Measurement of gain for optimum bias current and flux bias as a function of frequency. The V–Φ curves at an optimal bias current of 16 μA and the operating point is marked by red dot in the inset.

The power-handling capability of the amplifier is an important figure of merit, which determines the dynamic range of the amplifier. The input saturation power, as an evaluation of power-handling capability, was measured at the optimal operating point reported previously. As shown in Fig. 7, the 1-dB compression point, a standard metric for saturation power, occurs at an input power of approximately −115 dBm. This power-handling capability meets the requirements for most applications demanding near-quantum-limited amplification.

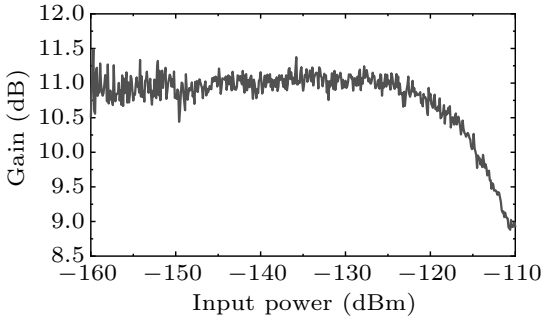


Fig. 7. The maximum gain at 5.39 GHz as a function of SQUID amplifier input power.

These measured results show good agreement with simulations in terms of operating frequency and bandwidth characteristics. However, we observed slight deviations that could be attributed to two primary factors. Firstly, in the SQUID-unit layout simulations, JJs were represented by the RCSJ model, which may not accurately capture the junction microwave characteristics. Secondly, the tolerances in the fabrication process can lead to variations in the actual parameters of the device, consequently affecting operational performance.

In addition, the noise performance is another critical metric for SQUID amplifiers, but it could not be directly measured due to experimental constraints. Therefore, we have theoretically estimated the device's noise temperature using the following expression:[21]

$$T_{\mathrm{N}}^{\mathrm{opt}} \approx \frac{7\omega_0 T}{V_\Phi},$$

where $\omega_0 = 5.39 \times 2\pi \times 10^9$ rad/s, $T = 4.2$ K, and $V_\Phi \sim 300\ \mu\mathrm{V}/\Phi_0$. Substituting the values into the equation yields a noise temperature of 6.86 K.

4. Conclusion

We have successfully designed and fabricated an SQUID microwave amplifier based on simulation tools and the Nb/Al–AlO_x/Nb trilayer junction process. The cryogenic characterization at 4.2 K demonstrates that the designed SQUID amplifier achieves a gain exceeding 10 dB at 5.39 GHz, a 3-dB bandwidth of 142 MHz, and a saturation power of approximately −115 dBm. The technological approach demonstrated here can be extended to the development of high-saturation-power Josephson parametric amplifiers.[15]

We observed slight deviations between the measured results and simulation predictions, and we will concentrate on two main aspects to improve: (i) optimizing the fabrication process to reduce manufacturing deviations, and (ii) replacing the lumped-element RCSJ model with a physics-based Josephson junction model to improve simulation fidelity.

Acknowledgements

Project supported by the National Natural Science Foundation of China (Grant No. 12273099) and the Shanghai Science and Technology Program (Grant No. 25LZ2600600).

The authors would like to thank all staff at the Superconducting Electronics Facility (SELF) of SIMIT for their assistance during the fabrications.

References

[1] Bradley R, Clarke J, Kinion D, *et al*. 2003 *Rev. Mod. Phys.* **75** 777
[2] Asztalos S J, Carosi G, Hagmann C, *et al*. 2010 *Phys. Rev. Lett.* **104** 041301
[3] Hagmann C, Kinion D, Stoeffl W, *et al*. 1998 *Phys. Rev. Lett.* **80** 2043
[4] Boyd S T P and De Haan T 2025 *IEEE Trans. Appl. Supercond.* **35** 3530377
[5] Chen Y Y, Wang C Q, Xu Y X, *et al*. 2023 *Chin. Phys. B* **32** 118501
[6] Michotte S 2009 *Appl. Phys. Lett.* **94** 122511
[7] Serban I, Plourde B L T and Wilhelm F K 2008 *Phys. Rev. B* **78** 054507
[8] Lupascu A, Driessen E F C, Roschier L, *et al*. 2006 *Phys. Rev. Lett.* **96** 127003
[9] Schupp F J, Vigneau F, Wen Y, *et al*. 2020 *J. Appl. Phys.* **127** 244503
[10] Mück M, Kycia J B and Clarke J 2001 *Appl. Phys. Lett.* **78** 967
[11] Hilbert C and Clarke J 1985 *J. Low Temp. Phys.* **61** 263
[12] Zheng Y, Xiong K, Feng J, *et al*. 2024 *Chin. Phys. B* **33** 020701
[13] Castellanos-Beltran M A, Irwin K D, Hilton G C, *et al*. 2008 *Nat. Phys.* **4** 929
[14] Planat L, Dassonneville R, Puertas Martínez J, *et al*. 2019 *Phys. Rev. Appl.* **11** 034014
[15] Kaufman R, White T, Dykman M I, *et al*. 2023 *Phys. Rev. Appl.* **20** 054058
[16] Wallraff A, Schuster D I, Blais A, *et al*. 2004 *Nature* **431** 162
[17] Defeo M P, Bhupathi P, Yu K, *et al*. 2010 *Appl. Phys. Lett.* **97** 092502
[18] Defeo M P and Plourde B L T 2012 *Appl. Phys. Lett.* **101** 052603
[19] Wu W, Lin Z, Ni Z, *et al*. 2024 *J. Low Temp. Phys.* **214** 143
[20] Ying L Y, Zhang X Y, Niu M Y, *et al*. 2021 *IEEE Trans. Appl. Supercond.* **31** 1300105
[21] Mück M and Mcdermott R 2010 *Supercond. Sci. Technol.* **23** 093001